Supplementary Information

Electronic structure engineering and cascade electron transfer channel in Ni_2P/1T-WS_2/$ZnIn_2S_4$ ternary heterojunction for enhanced photocatalytic hydrogen evolution: Construction, kinetics, and mechanistic insights

Hua Lv [a], Zhiyun Suo [a], Fubiao Zhang [a], Baoliang Wan [a], Chayuan Zhou [a], Xinyan Xing [a], Gongke Wang [b,*], Yuehua Chen [a,*], Yumin Liu [a,*]

[a] Collaborative Innovation Center of Henan Province for Green Manufacturing of Fine Chemicals, Key Laboratory of Green Chemical Media and Reactions, Ministry of Education, School of Chemistry and Chemical Engineering, Henan Normal University, Xinxiang, Henan 453007, China.

[b] School of Materials Science and Engineering, Henan Engineering Research Center of Design and Recycle for Advanced Electrochemical Energy Storage Materials, Henan Normal University, Xinxiang, Henan 453007, China

*Corresponding author; E-mail: wanggongke@126.com (G Wang); 031124@htu.cn (Y Chen); ymliu2007@163.com (Y Liu)

Materials

Indium chloride ($InCl_3$, 99%) and thioacetamide (C_2H_5NS, TAA, 99%) were purchased from Shanghai Macklin Biochemical Technology Co., Ltd. Tungsten chloride (WCl_6, 99%) and red phosphorus (P, 98.5%) were supplied by Shanghai Aladdin Biochemical Technology Co., Ltd. Zinc chloride ($ZnCl_2$, 99%), nickel chloride hexahydrate ($NiCl_2 \cdot 6H_2O$, 99%) and N,N-dimethylformamide (C_3H_7NO, DMF, 99.5%) were obtained from Tianjin DeEn Chemical Reagent Co., Ltd. All chemicals utilized were of analytical grade and were applied as received.

Materials characterization

Morphological and elemental distribution measurements were conducted using a scanning electron microscope (SEM, JSM-6390-LV). A transmission electron microscope (TEM, JEM2100) was employed for lattice fringe and microstructure characterizations. X-ray diffraction (XRD) was conducted using a powder X-ray diffractometer (Bruker D8 Advance) equipped with Cu-Kα radiation. The optical properties were investigated using UV-Vis diffuse reflectance spectroscopy (DRS) with a Cary5000 UV-Vis-NIR spectrometer. The BET surface area analyses were carried out using a Micromeritics ASAP 2010 automated adsorption instrument. X-ray photoelectron spectroscopy (XPS) spectra were obtained using an ESCALAB MKII instrument. Ultraviolet photoelectron spectroscopy (UPS) characterizations were performed on an AXIS SUPRA+ instrument (KRATOS). The photoluminescence (PL) tests were carried out using an FLsp920 fluorescence spectrometer at an excitation wavelength of 475 nm. Raman spectroscopy was conducted on a LabRAM HR evolution spectrometer. A Malvern Nano-ZS90 Zetasizer was utilized to analyze the zeta potential of the products. Fourier transform infrared (FTIR) spectra were acquired a Spectrum 400F spectrometer with a spectral resolution of 4 cm^{-1}.

Electrochemical measurements

Photocurrent response, Mott-Schottky (MS), cyclic voltammetry (CV) and electrochemical impedance spectroscopy (EIS) measurements were performed using an electrochemical workstation (CHI-660D) with 0.5 M Na_2SO_4 solution as the electrolyte solution and the Ag/AgCl and Pt wires as the reference and counter electrodes, respectively. For the preparation of the working electrode, 5 mg of catalyst was suspended in a mixture consisting of 10 μL Nafion and 0.25 mL water, followed by sonication for 30 minutes to form a uniform slurry. The prepared slurry was deposited onto a 1 cm × 1 cm fluorine-doped tin oxide (FTO) glass substrate, followed by drying at 60 °C for 30 minutes. For the photocurrent measurements, a 300 W Xe lamp was utilized as the light source, while a 1 M KOH solution was used as the electrolyte in the linear sweep voltammetry (LSV) tests.

Photocatalytic experiments

The photocatalytic H_2 generation tests were carried out in a sealed Labsolar-III reactor (Perfectlight, Beijing). Typically, 50 mg catalyst was dispersed in 100 mL of aqueous solution comprising 10 % lactic acid. Prior to irradiation with a 300 W xenon lamp, the quartz reactor was purged with high-purity N_2 for 30 minutes and then evacuated to remove residual air. The reactant solution was irradiated with the xenon lamp while being magnetically stirred, with the temperature held constant at 25 °C. At specific intervals, the hydrogen evolved was quantified by on-line gas chromatography (GC-7900), employing nitrogen as the carrier gas. The apparent quantum efficiency (AQE) was determined using the following formula:

$$\text{AQE} = \frac{2 \times number\ of\ evolved\ H_2\ molecules}{number\ of\ incident\ photons}$$

Figures

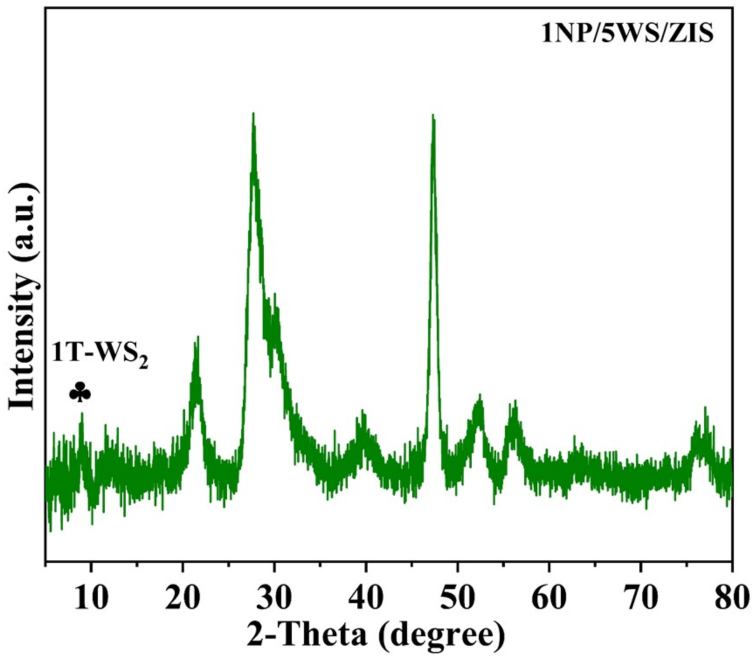

Fig. S1. XRD pattern of the 1NP/5WS/ZIS composite.

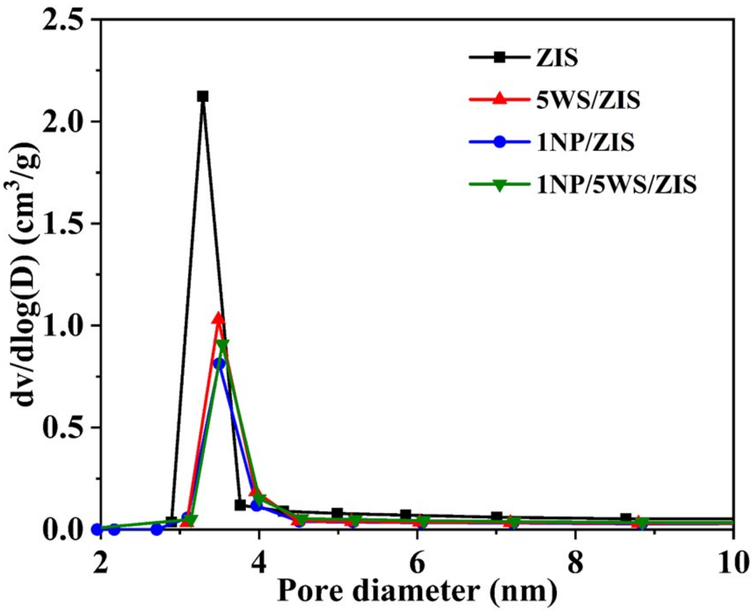

Fig. S2. Corresponding pore size distribution curves of the ZIS, 5WS/ZIS, 1NP/ZIS, and 1NP/5WS/ZIS samples.

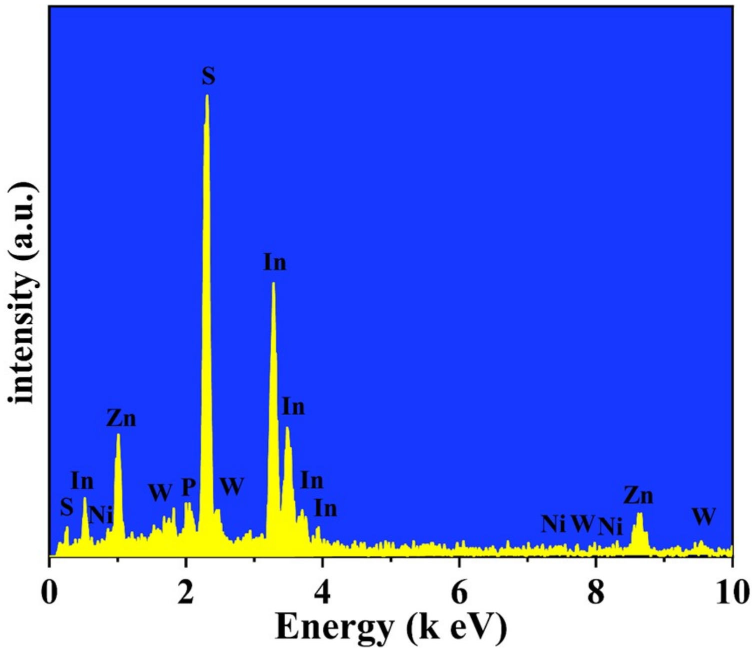

Fig. S3. Energy dispersive X-ray (EDX) spectrum of the 1NP/5WS/ZIS catalyst.

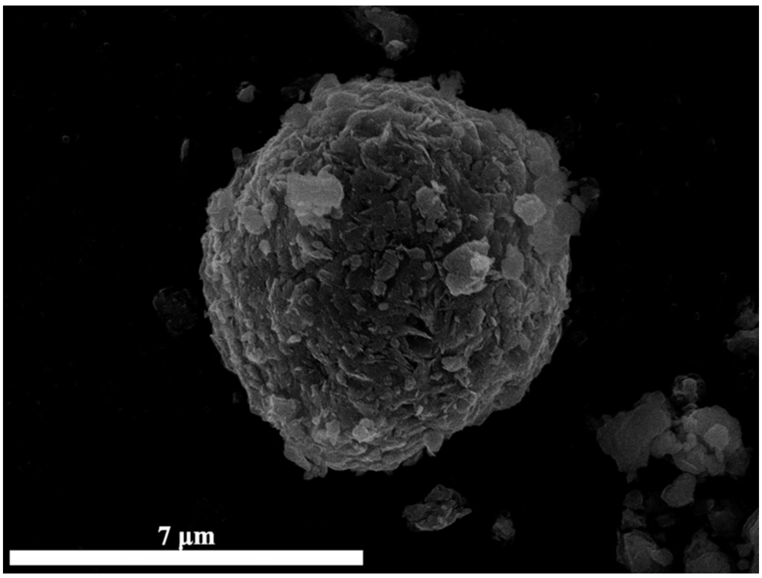

Fig. S4. Selected scanning region of EDX spectral analysis.

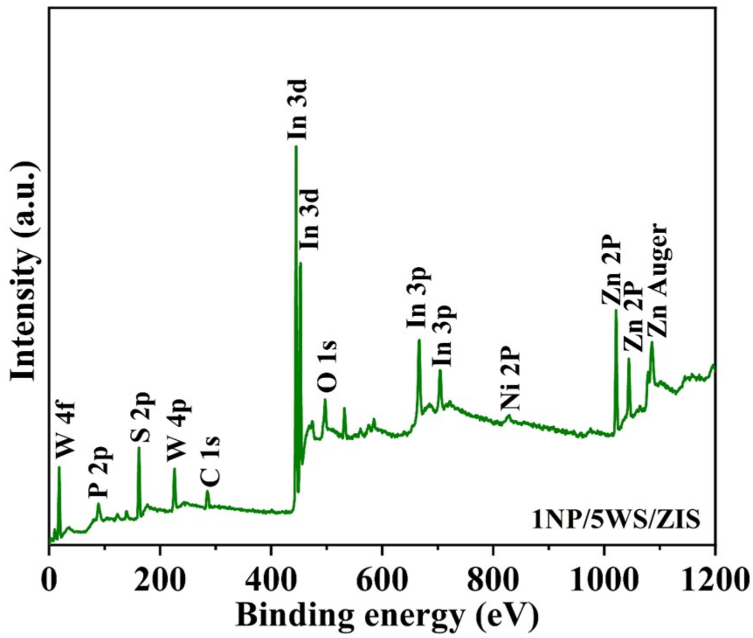

Fig. S5. Survey XPS spectrum of the 1NP/5WS/ZIS catalyst.

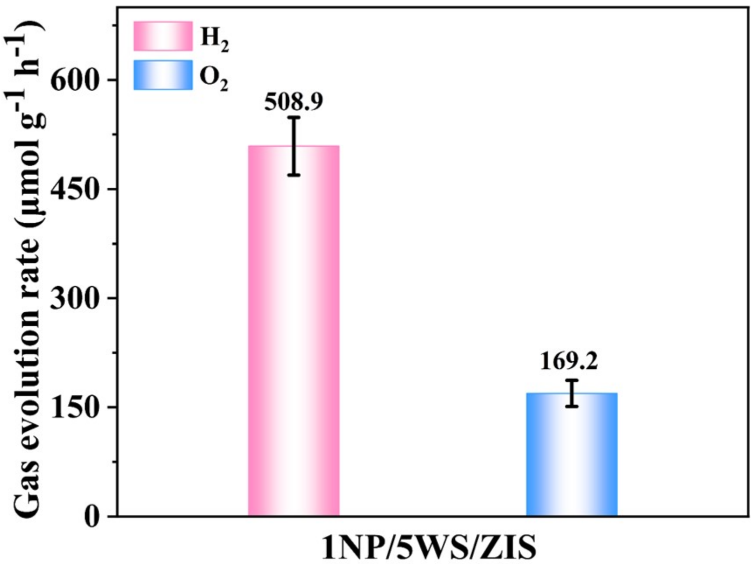

Fig. S6. Photocatalytic activity of pure water splitting of the 1NP/5WS/ZIS catalyst.

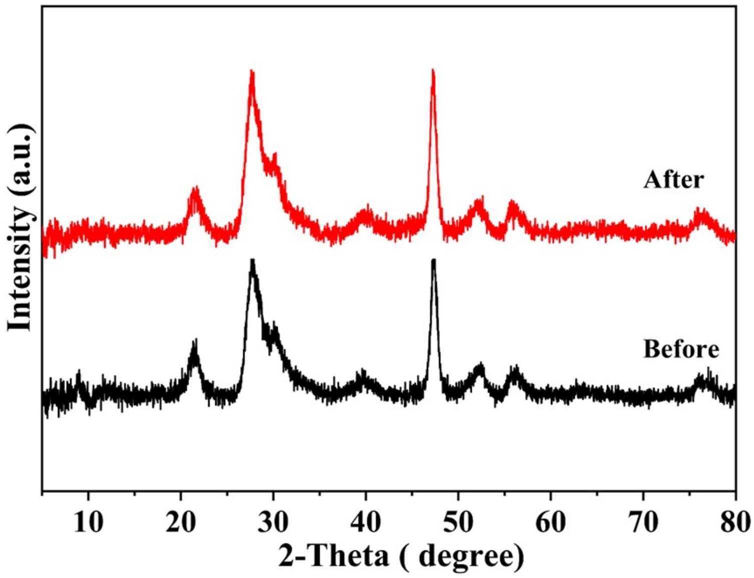

Fig. S7. XRD analysis of the 1NP/5WS/ZIS product before and after cycling tests.

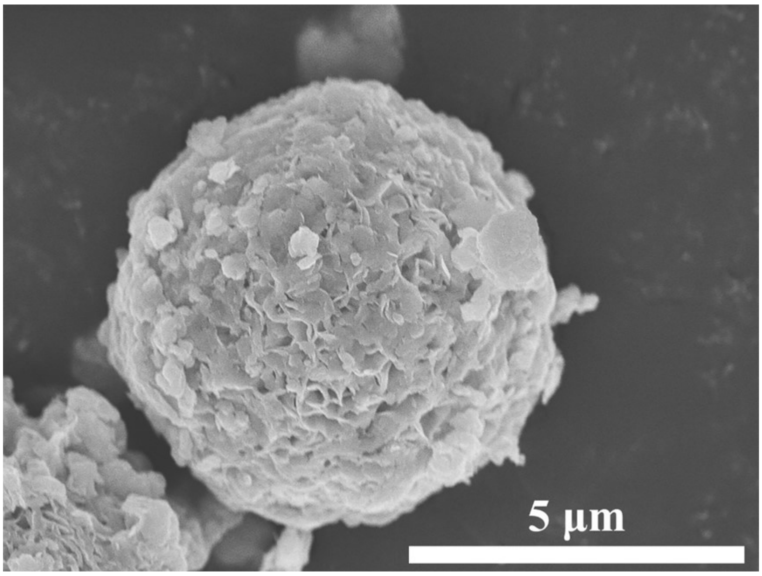

Fig. S8. SEM image of the 1NP/5WS/ZIS product after the cycling test.

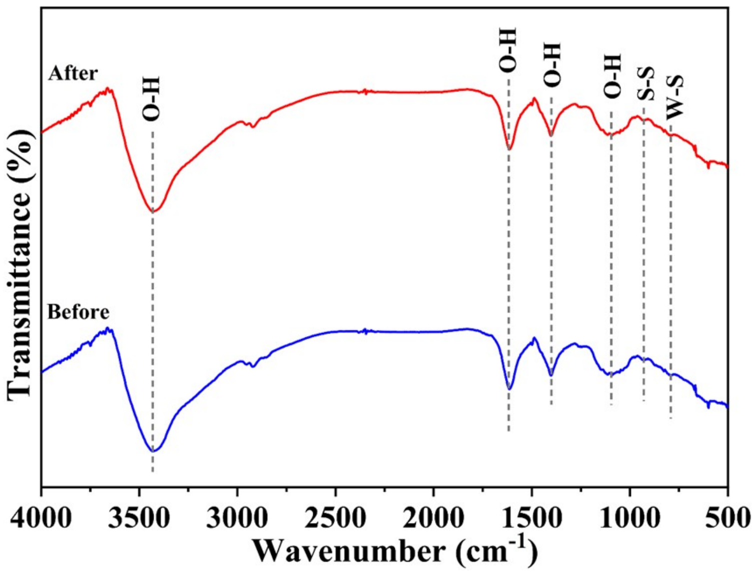

Fig. S9. FTIR spectra of the 1NP/5WS/ZIS product before and after cycling tests.

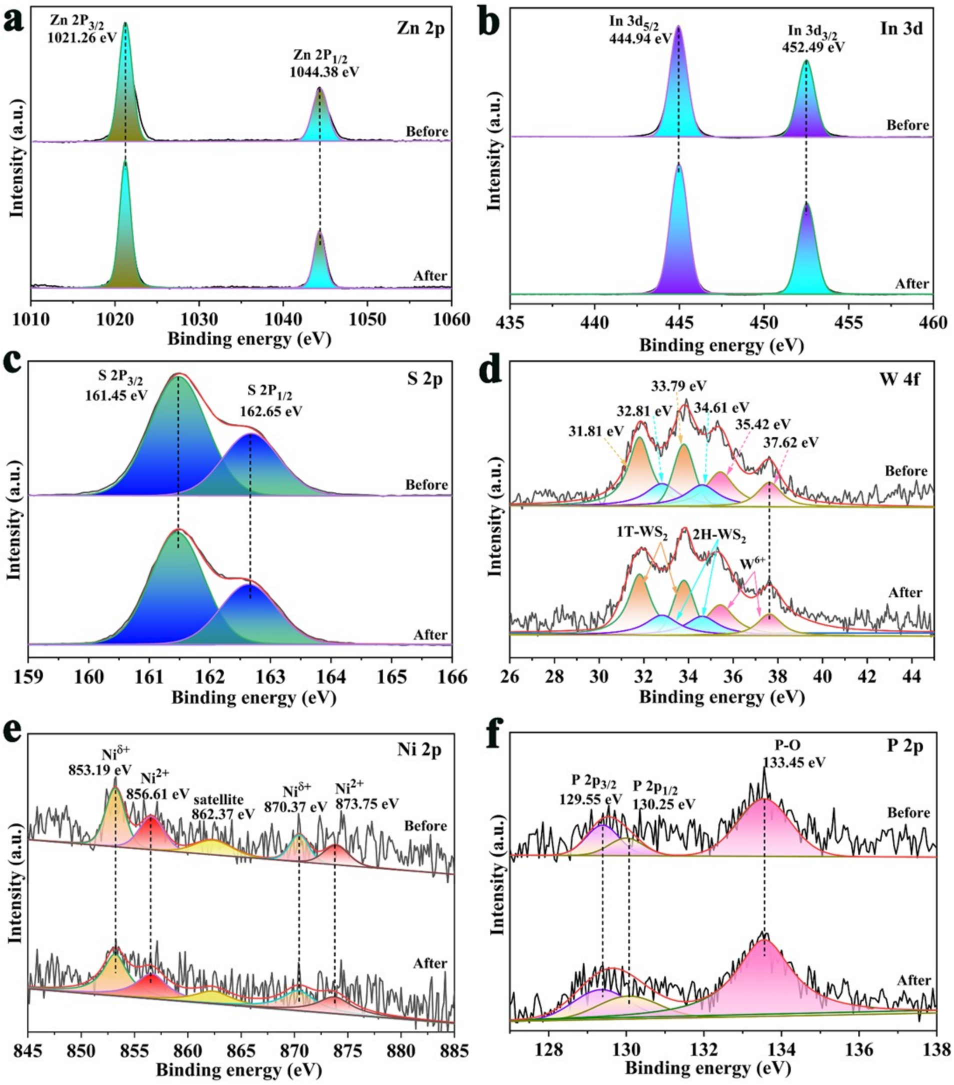

Fig. S10. XPS spectra of the 1NP/5WS/ZIS product before and after cycling tests: Zn 2p (a), In 3d (b), S 2p (c), W 4f (d), Ni 2p (e), and P 2p (f).

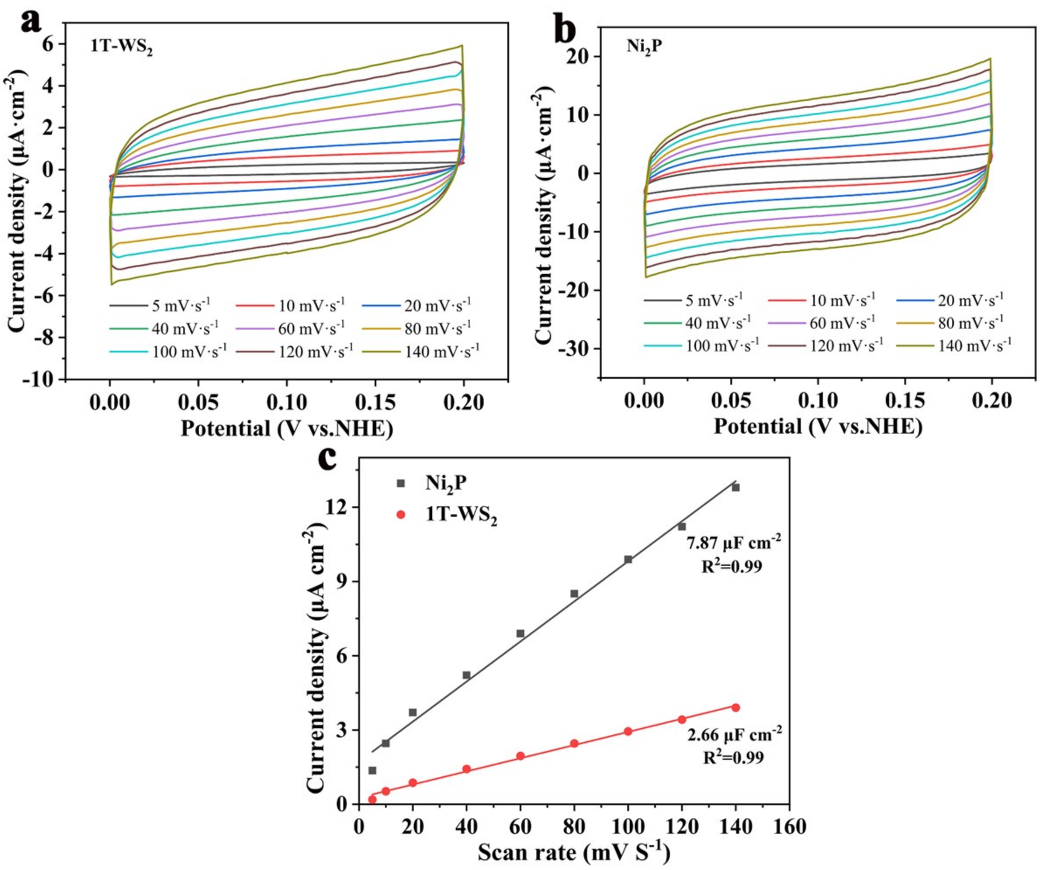

Fig.S11. CV curves (a-b) and current density versus scan rate fitting curves (c) of 1T-WS_2 and Ni_2P cocatalysts.

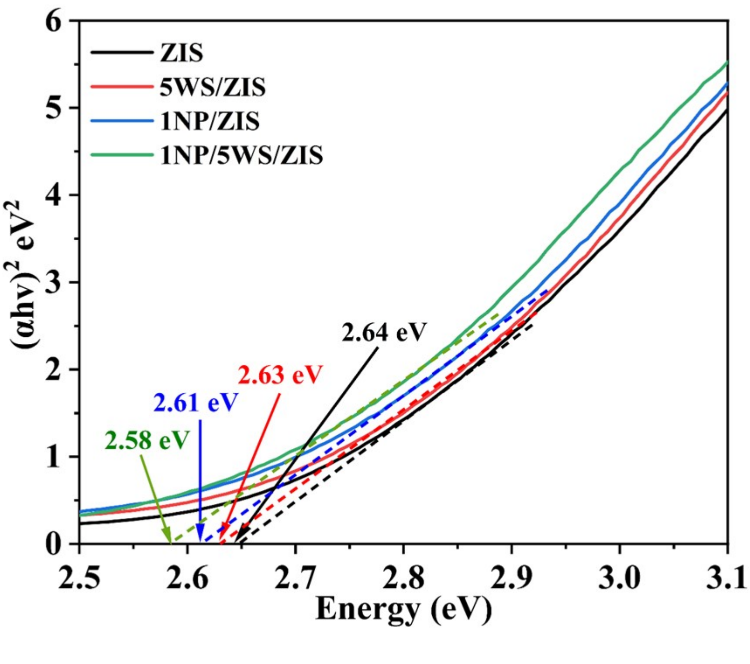

Fig. S12. Tauc plots of the ZIS, 5WS/ZIS, 1NP/ZIS, and 1NP/5WS/ZIS.

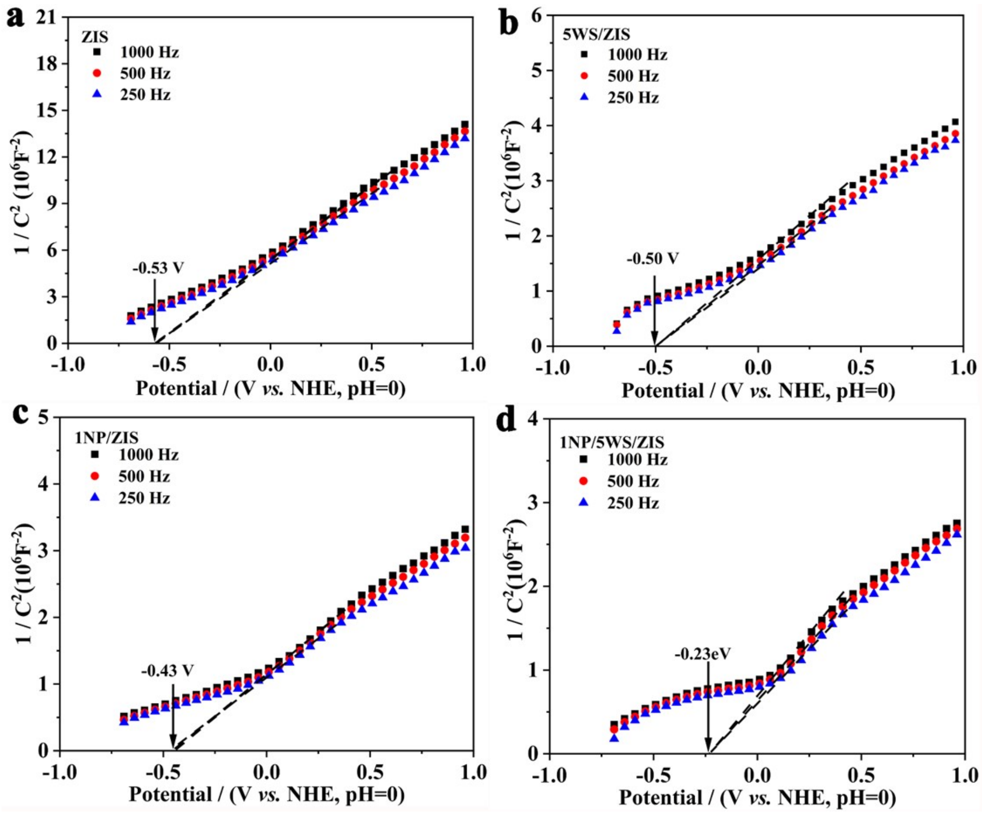

Fig. S13. MS curves of the ZIS (a), 5WS/ZIS (b), 1NP/ZIS (c), and 1NP/5WS/ZIS (d).

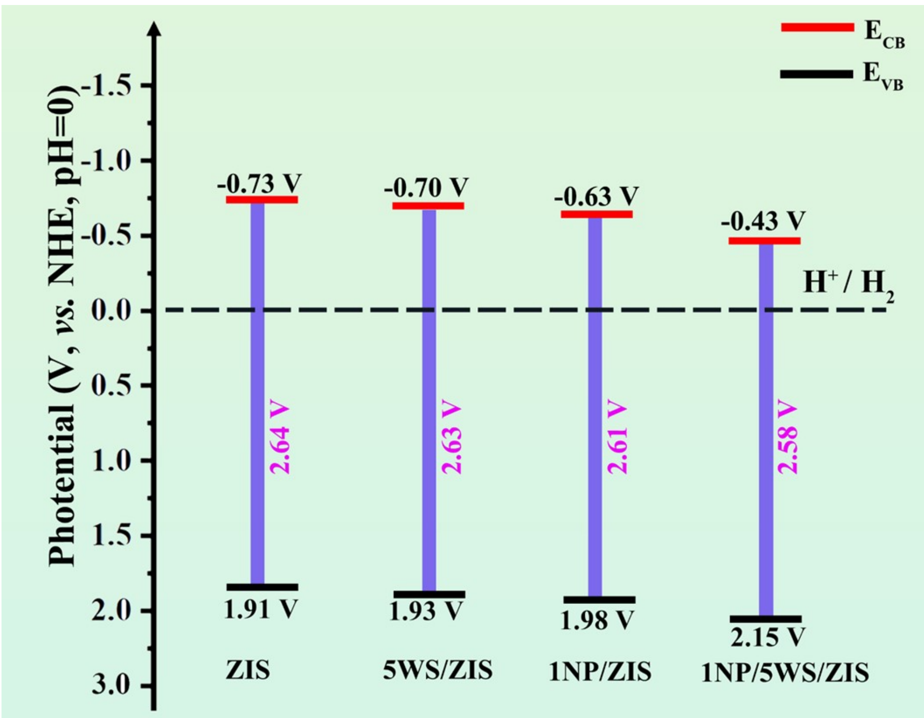

Fig. S14. Band structures variation of ZIS after the coupling with Ni_2P and 1T-WS_2 cocatalysts.

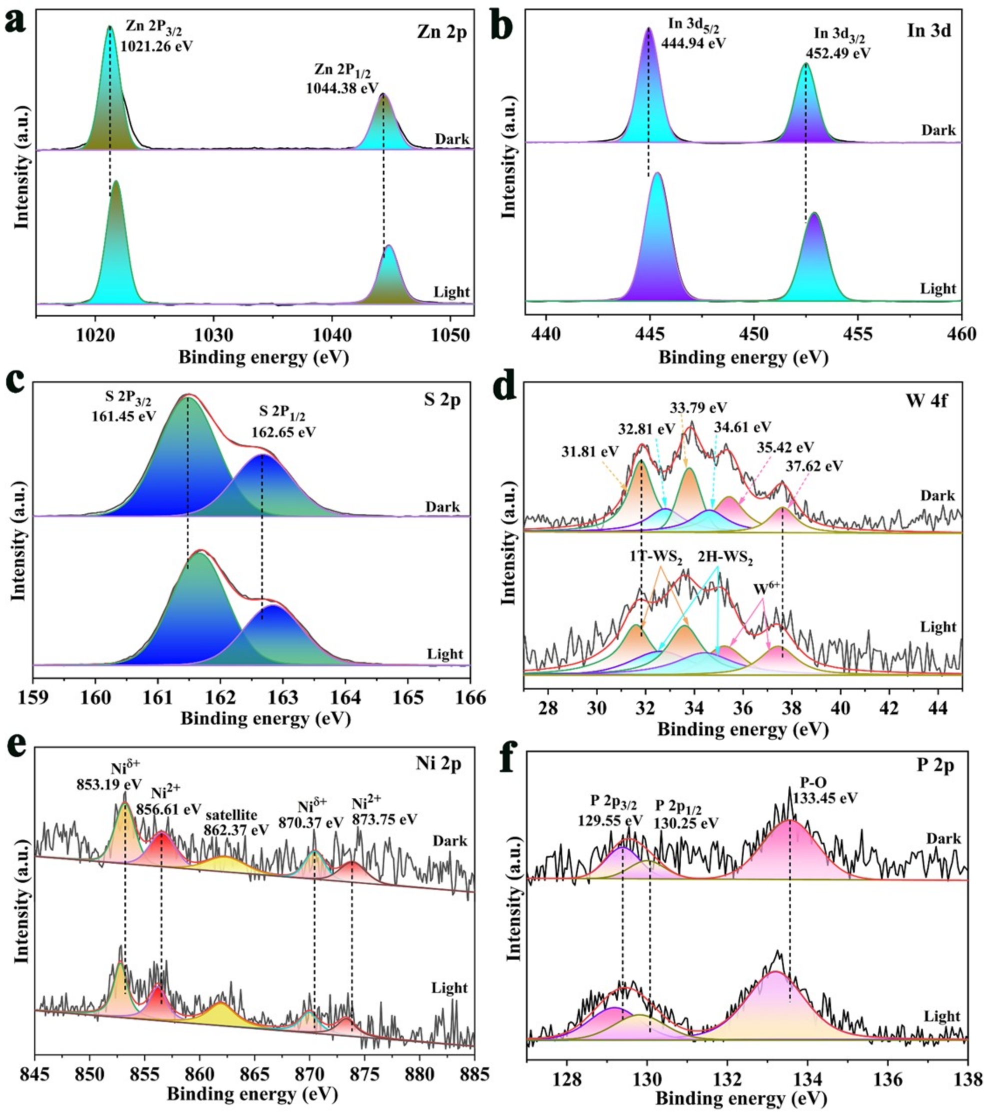

Fig. S15. XPS spectra of the Zn 2p (a), In 3d (b), S 2p (c), W 4f (d), Ni 2p (e), and P 2p (f) of the 1NP/5WS/ZIS in the dark or under 300W Xe lamp irradiation.

Tables

Table S1 Textural properties of the ZIS, 5WS/ZIS, 1NP/ZIS, and 1NP/5WS/ZIS catalysts.

Photocatalysts	BET surface area (m^2 g^{-1})	Average pore diameter (nm)	total pore volume (cm^3 g^{-1})
ZIS	98.97	8.33	0.214
5WS/ZIS	61.88	7.83	0.124
1NP/ZIS	50.85	7.72	0.095
1NP/5WS/ZIS	60.65	7.27	0.111

Table S2 Comparison of photocatalytic H_2 production rate of cocatalyst-assisted $ZnIn_2S_4$ systems.

Photocatalyst	Light source	Sacrificial agent	H_2 rate (mmol g^{-1} h^{-1})	Ref. (Year)
$MoS_2/ZnIn_2S_4$	300 W Xe-lamp λ ≥ 420 nm	lactic acid (12.5 vol%)	4.19	[S1] (2017)
MoS_2/CQDs/$ZnIn_2S_4$	300 W Xe-lamp λ ≥ 420 nm	0.1 M Na_2S/Na_2SO_3	3.00	[S2] (2018)
$In(OH)_3/ZnIn_2S_4$	300 W Xe-lamp λ ≥ 420 nm	Na_2S (0.35 M) Na_2SO_3 (0.25 M)	0.52	[S3] (2019)
$Co_9S_8/ZnIn_2S_4/PdS$	300 W Xe lamp λ > 420 nm	TEOA (25 vol%)	11.41	[S4] (2021)
$Co_2P/ZnIn_2S_4$	300 W Xe lamp	Na_2S (0.35 M) Na_2SO_3 (0.25 M)	7.93	[S5] (2021)
biochar/$ZnIn_2S_4$	150 W Xe-lamp AM 1.5 G filter	lactic acid (20 vol%)	4.47	[S6] (2022)
$NiO/ZnIn_2S_4$	300 W Xe-lamp λ ≥ 420 nm	TEOA (20 vol%)	5.00	[S7] (2023)
$ReS_2/ZnIn_2S_4$	four 3-W 420 nm LED lamps	lactic acid (10 vol%)	2.24	[S8] (2023)
1T-$MoS_2/ZnIn_2S_4$	300 W Xe-lamp AM 1.5 G filter	lactic acid (20 vol%)	15.60	[S9] (2024)
$ZnIn_2S_4/Co_9S_8/Ni_2P$	300 W Xe lamp λ > 420 nm	TEOA (20 vol%)	6.82	[S10] (2024)
MoO_2/C/$ZnIn_2S_4$	300 W Xe lamp λ > 420 nm	TEOA (10 vol%)	2.36	[S11] (2024)
$CoSe_2$/Na-$ZnIn_2S_4$	300 W Xe-lamp λ > 420 nm	TEOA (25 vol%)	4.53	[S12] (2024)
Ni_2P/1T-$WS_2/ZnIn_2S_4$	300 W Xe-lamp	lactic acid (10 vol%)	16.39	Present work

References

[S1] B. Chai, C. Liu, C. Wang, J. Yan, Z. Ren, Photocatalytic hydrogen evolution activity over $MoS_2/ZnIn_2S_4$ microspheres, Chinese Journal of Catalysis, 38 (2017) 2067-2075.

[S2] B. Wang, Z. Deng, X. Fu, Z. Li, MoS_2/CQDs obtained by photoreduction for assembly of a ternary MoS_2/CQDs/$ZnIn_2S_4$ nanocomposite for efficient photocatalytic hydrogen evolution under visible light, Journal of Materials Chemistry, A 6 (2018) 19735-19742.

[S3] M. Geng, Y. Peng, Y. Zhang, X. Guo, F. Yu, X. Yang, G. Xie, W. Dong, C. Liu, J. Li, J. Yu, Hierarchical $ZnIn_2S_4$: A promising cocatalyst to boost visible-light-driven photocatalytic hydrogen evolution of $In(OH)_3$, International Journal of Hydrogen Energy, 44 (2019) 5787-5798.

[S4] M. Wang, G. Zhang, Z. Guan, J. Yang, Q. Li, Spatially Separating Redox Centers and Photothermal Effect Synergistically Boosting the Photocatalytic Hydrogen Evolution of $ZnIn_2S_4$ Nanosheets, Small, 17 (2021) e2006952.

[S5] Q. Zhang, X. Wang, J. Zhang, L. Li, H. Gu, W.L. Dai, Hierarchical fabrication of hollow Co_2P nanocages coated with $ZnIn_2S_4$ thin layer: Highly efficient noble-metal-free photocatalyst for hydrogen evolution, J Colloid Interface Sci, 590 (2021) 632-640.

[S6] P. Bhavani, D. Praveen Kumar, M. Hussain, T.M. Aminabhavi, Y. K. Park, Eco-friendly rice husk derived biochar as a highly efficient noble Metal-Free cocatalyst for high production of H_2 using solar light irradiation, Chemical Engineering Journal, 434 (2022) 134743.

[S7] Y. Wang, J. Ye, B. Hu, Y. Xie, Y. Ling, Z. Wang, Y. Chen, NiO co-catalyst modification $ZnIn_2S_4$ driving efficient hydrogen generation under visible light, Separation and Purification Technology, 320 (2023) 124096.

[S8] J. Xu, W. Zhong, F. Chen, X. Wang, H. Yu, In situ cascade growth-induced strong coupling effect toward efficient photocatalytic hydrogen evolution of $ReS_2/ZnIn_2S_4$, Applied Catalysis B: Environmental, 328 (2023) 122493.

[S9] Y. Ji, X. Ding, Y. Xue, J. Wang, J. Tian, Metallic 1T phase molybdenum disulfide cocatalyst with abundant edge and substrate active sites for enhanced photocatalytic hydrogen production activity of zinc indium sulfide nanoflowers, J Colloid Interface Sci, 654 (2024) 1340-1347.

[S10] Y. H. Wu, Y. Q. Yan, Y. Wei, J. Wang, A. Li, W. Y. Huang, J. L. Zhang, K. Yang, K. Q. Lu, Decorating $ZnIn_2S_4$ with earth-abundant Co_9S_8 and Ni_2P dual cocatalysts for boosting photocatalytic hydrogen evolution, International Journal of Hydrogen Energy, 78 (2024) 452-459.

[S11] X. Zhang, H. Ye, Z. Zeng, K. Sa, J. Jia, Z. Yang, S. Xu, C. Han, Y. Liang, Bridging the gap between metallic MoO_2 and $ZnIn_2S_4$ for enhanced photocatalytic H_2 production, Separation and Purification Technology, 347 (2024) 127624.

[S12] S. Yuan, G. Liu, Q. Zhang, T. Liu, J. Yang, Z. Guan, Synergistic effect of Na doping and $CoSe_2$ cocatalyst for enhanced photocatalytic hydrogen evolution performance of $ZnIn_2S_4$, J Colloid Interface Sci, 676 (2024) 272-282.